

A Modified Spherical Model of a First-Order Phase Transition*

J. S. LANGER

Physics Department, Carnegie Institute of Technology, Pittsburgh, Pennsylvania

(Received 25 September 1964)

It is shown that the addition of a weak anisotropy field to the spherical model produces a very complete and realistic mathematical picture of a first-order phase transition. In contrast to the conventional spherical model of a ferromagnet (or lattice gas), the modified model exhibits phase separation in the flat two-phase region of the magnetization curve (or isotherm). The magnetization curve has an analytic continuation into the two-phase region which may be identified with a homogeneous metastable state. The new model is not exactly soluble but lends itself easily to a diagram renormalization technique. Except in the immediate neighborhood of the critical point, this technique gives rigorous results.

I. INTRODUCTION

THE spherical model of a ferromagnet¹ or lattice gas^{2,3} is probably the most satisfactory model of a first-order phase transition proposed to date. It is a three-dimensional model in which the spins or particles interact via finite range forces. It is exactly soluble in an external magnetic field; that is, one may compute complete isotherms for the equivalent lattice gas. Thus the spherical model is more realistic than either Temperley's infinite-dimensional (infinite-range) model⁴⁻⁷ or the hard-rod model of Kac, Uhlenbeck, and Hemmer,⁸ which is one dimensional and requires infinite range forces to produce a phase transition. It is more completely soluble than the two-dimensional Ising model.^{9,10}

It is all the more disappointing, therefore, that the spherical model does not give a satisfactory description of condensation. As we see in the discussion below, the model does not properly describe the physical separation of two phases in equilibrium. A related difficulty is that the spherical model apparently does not exhibit supersaturation. It is commonly supposed that the analytic continuation of the magnetization curve—the van der Waals loop in the isotherm—describes a metastable state. No suitable analytic continuation occurs for the spherical model.

The present paper describes an attempt to make a virtue of the above faults by showing that if one modifies the spherical model in such a way as to encourage phase separation, one also recovers supersaturation. This constitutes a partial verification of the classic phenomenological theories of condensation and metastability.¹¹ More important, the new model pro-

vides an extremely detailed mathematical picture of the phase transition, even throwing some light on the nature of the mathematical difficulties near the critical point. The new model involves the addition of a small quartic perturbation which plays the role of an anisotropy field. Although not exactly soluble, it is sufficiently simple that many conclusions may be drawn with confidence.

Sections II and III of this paper are devoted to a critical review of the spherical model and a qualitative justification for the proposed modification. In Sec. II we reproduce the well-known solution of the spherical model and emphasize the fact that the differential susceptibility at zero field diverges below the transition temperature, thus precluding a smooth transition to a metastable phase. Some relevant but rather detailed properties of the partition function for the pure spherical model are discussed in Appendix A. Then, in Sec. III, we argue that the lack of a metastable phase is connected with the lack of phase separation in the two-phase system, and illustrate this unphysical property of the spherical model by a simple zero-temperature calculation. Finally, it is shown that the quartic perturbation restores phase separation, at least at zero temperature. The nonlinear differential equation which appears here and in Sec. VII is discussed in Appendix B.

A perturbation-theoretic formalism for investigation of the modified model is developed in Secs. IV and V. It is clear that the partition function has a singularity where the strength of the quartic perturbation vanishes. Accordingly, instead of a direct expansion, we write the partition function as an integral over a variable z (the same variable which enters the pure spherical model in the role of a chemical potential), and make a linked-cluster expansion of the logarithm of this integrand in powers of the perturbation. The rules for this expansion are developed in Sec. IV. In Sec. V, we renormalize this expansion. The renormalized variables turn out to be the magnetization and the spin-spin correlation function, which plays the role of a propagator. Some very useful variational properties of the renormalized expansion are also discussed in Sec. V.

The thermodynamic properties of the modified spherical model are presented in Secs. VI and VII. We find that for a sufficiently small perturbation

* Supported in part by the National Science Foundation.

¹ T. H. Berlin and M. Kac, *Phys. Rev.* **86**, 821 (1952).

² W. Pressman and J. B. Keller, *Phys. Rev.* **120**, 22 (1960).

³ H. A. Gersch and T. H. Berlin, *Phys. Rev.* **127**, 2276 (1962).

⁴ H. N. V. Temperley, *Proc. Phys. Soc. (London)* **A67**, 233 (1954).

⁵ S. Katsura, *Progr. Theoret. Phys. (Kyoto)* **13**, 571 (1955).

⁶ N. Saito, *J. Chem. Phys.* **35**, 232 (1961).

⁷ C. Bloch and J. S. Langer, *J. Math. Phys.* (to be published).

⁸ M. Kac, G. E. Uhlenbeck, and P. C. Hemmer, *J. Math. Phys.* **4**, 216 and 229 (1963).

⁹ L. Onsager, *Phys. Rev.* **65**, 117 (1944); B. Kaufmann, *ibid.* **76**, 1232 (1949).

¹⁰ C. N. Yang, *Phys. Rev.* **85**, 809 (1952).

¹¹ For example, see J. Frenkel, *Kinetic Theory of Liquids* (Dover Publications, Inc., New York, 1955), Chap. 7.

strength and for temperatures not in the immediate vicinity of the critical point, it is sufficient to keep only the first-order term in the renormalized expansion. The magnetization curve is computed in Sec. VI. The important point is that the curve now has a smooth continuation into what may be interpreted as a region of metastability. The validity of the calculation is established by a self-consistency check. In Sec. VII we deal with the two-phase region. It is shown that the canonical free energy is a convex function of magnetization and has a flat section corresponding to two separated phases in equilibrium. The shape of the surface between the two phases is computed.

II. PROPERTIES OF THE SPHERICAL MODEL

We consider a lattice of N sites, labeled by the index \mathbf{l} , each occupied by a spin $\mu_{\mathbf{l}}$. As usual, the spin states will satisfy periodic boundary conditions. The interaction between the spins is given by

$$H_0 = -\frac{1}{2} \sum_{\mathbf{l}, \mathbf{l}'} v_{\mathbf{l}, \mathbf{l}'} \mu_{\mathbf{l}} \mu_{\mathbf{l}'} \tag{2.1}$$

The spherical model differs from the Ising model in that the spin variables $\mu_{\mathbf{l}}$ are allowed to take on all real values ($-\infty < \mu_{\mathbf{l}} < \infty$) subject to the "spherical constraint":

$$\sum_{\mathbf{l}} \mu_{\mathbf{l}}^2 = N. \tag{2.2}$$

Statistical averages are to be performed over this N -dimensional hypersphere in μ space. This model exhibits a phase transition only in three or more dimensions. Accordingly, all further discussion pertains to a three-dimensional system.

In the following work, we are interested in both the canonical partition function,

$$\Xi_0(m) = \frac{1}{A_N} \prod_{\mathbf{l}} \left(\int_{-\infty}^{\infty} d\mu_{\mathbf{l}} \right) \delta \left(\sum_{\mathbf{l}} \mu_{\mathbf{l}}^2 - N \right) \times \delta \left(\sum_{\mathbf{l}} \mu_{\mathbf{l}} - mN \right) e^{-\beta H_0}, \tag{2.3}$$

and the grand canonical partition function

$$Z_0(\lambda) = \frac{1}{A_N} \prod_{\mathbf{l}} \left(\int_{-\infty}^{\infty} d\mu_{\mathbf{l}} \right) \delta \left(\sum_{\mathbf{l}} \mu_{\mathbf{l}}^2 - N \right) \times \exp \left\{ -\beta H_0 + \lambda \sum_{\mathbf{l}} \mu_{\mathbf{l}} \right\} = N \int_{-1}^1 \Xi_0(m) e^{\lambda N m} dm. \tag{2.4}$$

Conventionally, the normalization factor A_N is taken to be the area of the hypersphere:

$$A_N = 2\pi^{N/2} N^{1/2(N-1)} / \Gamma(\frac{1}{2}N). \tag{2.5}$$

At this point, we review the evaluation of both of these partition functions. The techniques are well known but some of the details are required for use below.

In order to reduce (2.3) or (2.4) to an analytic form, we use an integral representation of the delta function

$$\delta \left(\sum_{\mathbf{l}} \mu_{\mathbf{l}}^2 - N \right) = \frac{\beta}{2\pi i} \int_{-i\infty}^{i\infty} dz \exp \left\{ N\beta z - \beta z \sum_{\mathbf{l}} \mu_{\mathbf{l}}^2 \right\}. \tag{2.6}$$

With this insertion, we obtain, in the integrand, an exponential of the following quadratic form in the $\mu_{\mathbf{l}}$'s:

$$\sum_{\mathbf{l}, \mathbf{l}'} P_{\mathbf{l}, \mathbf{l}'} \mu_{\mathbf{l}} \mu_{\mathbf{l}'} \equiv \sum_{\mathbf{l}, \mathbf{l}'} (z\delta_{\mathbf{l}, \mathbf{l}'} - \frac{1}{2}v_{\mathbf{l}, \mathbf{l}'}) \mu_{\mathbf{l}} \mu_{\mathbf{l}'}. \tag{2.7}$$

Because $v_{\mathbf{l}, \mathbf{l}'}$ is a function only of $\mathbf{l} - \mathbf{l}'$ for a translationally symmetric lattice, P may be diagonalized by the Fourier transformation

$$\mu_{\mathbf{l}} = \sum'_{\mathbf{k}, s=1,2} a_s(\mathbf{l}, \mathbf{k}) \sigma_{\mathbf{k}, s}, \tag{2.8}$$

where

$$\begin{aligned} a_1(\mathbf{l}, \mathbf{0}) &= 1/N^{1/2}, \\ a_1(\mathbf{l}, \mathbf{k}) &= (2/N)^{1/2} \cos \mathbf{k} \cdot \mathbf{l}, \quad \mathbf{k} \neq \mathbf{0}, \\ a_2(\mathbf{l}, \mathbf{k}) &= (2/N)^{1/2} \sin \mathbf{k} \cdot \mathbf{l}, \end{aligned} \tag{2.9}$$

and the notation \sum' implies that the sum is to be taken over only half of the allowed \mathbf{k} 's in the Brillouin zone plus $\mathbf{k} = \mathbf{0}$. More precisely, if $+\mathbf{k}$ is included in the sum, $-\mathbf{k}$ is not. The reader may check that (2.8) is an orthogonal transformation.

Now consider $Z_0(\lambda)$. We transform to the variables σ and perform the integrations as follows:

$$\begin{aligned} Z_0(\lambda) &= \frac{\beta}{2\pi i A_N} \prod_{\mathbf{l}} \left(\int_{-\infty}^{\infty} d\mu_{\mathbf{l}} \right) \int_{-i\infty}^{i\infty} dz \exp \left\{ N\beta z - \beta \sum_{\mathbf{l}, \mathbf{l}'} P_{\mathbf{l}, \mathbf{l}'} \mu_{\mathbf{l}} \mu_{\mathbf{l}'} + \lambda \sum_{\mathbf{l}} \mu_{\mathbf{l}} \right\} \\ &= \frac{\beta}{2\pi i A_N} \int_{-i\infty}^{i\infty} dz \prod'_{\mathbf{k}, s=1,2} \left(\int_{-\infty}^{\infty} d\sigma_{\mathbf{k}, s} \right) \exp \left\{ N\beta z - \beta \sum'_{\mathbf{k}, s} p_{\mathbf{k}} \sigma_{\mathbf{k}, s}^2 + N^{1/2} \lambda \sigma_{\mathbf{0}, 1} \right\} \\ &= \frac{\beta}{4\pi i} e^{-N/2} (2\beta)^{-N/2} \int_{-i\infty}^{i\infty} dz \exp \{ NF(z, \lambda) \}. \end{aligned} \tag{2.10}$$

Here,

$$F(z, \lambda) = \beta z - (1/2N) \sum_{\mathbf{k}} \ln p_{\mathbf{k}} + (\lambda^2/4\beta p_0), \quad (2.11)$$

where the $p_{\mathbf{k}}$'s are the eigenvalues of $P_{1,1'}$:

$$p_{\mathbf{k}} = z - (v_{\mathbf{k}}/2); \quad (2.12)$$

and the $v_{\mathbf{k}}$'s are the coefficients of the Fourier expansion

$$v_{1,1'} = (1/N) \sum_{\mathbf{k}} v_{\mathbf{k}} e^{i\mathbf{k} \cdot (1-1')}. \quad (2.13)$$

The final integral in (2.10) may be evaluated by a saddle-point technique. Note first that $F(z, \lambda)$ has a branch cut extending to the left from the branch point at $z = \frac{1}{2}v_{\max}$. For simplicity, let us assume that $v_{\mathbf{k}}$ is a real function, that the largest $v_{\mathbf{k}} = v_{\max}$ occurs at $\mathbf{k} = 0$, and that, near $\mathbf{k} = 0$, $v_{\mathbf{k}}$ may be expanded in the form

$$v_{\mathbf{k}} = v_0 - \gamma k^2 + \dots \quad (2.14)$$

It follows then that, near $z = v_0/2$, the singular function in F admits the expansion

$$\begin{aligned} \frac{1}{2N} \sum_{\mathbf{k}} \ln p_{\mathbf{k}} &= \frac{1}{2N} \sum_{\mathbf{k}} \ln(z - \frac{1}{2}v_{\mathbf{k}}) \\ &= A + B(z - \frac{1}{2}v_0) - C(z - \frac{1}{2}v_0)^{3/2} \\ &\quad + (z - \frac{1}{2}v_0)^2 \varphi(z), \end{aligned} \quad (2.15)$$

where B and C are positive coefficients

$$B = (1/N) \sum_{\mathbf{k}} [1/(v_0 - v_{\mathbf{k}})], \quad (2.16)$$

$$C = (1/3\pi\gamma)(2/\gamma)^{1/2}, \quad (2.17)$$

and φ is a function which is analytic at $z = v_0/2$.

The saddle-point equation is

$$\left. \frac{dF}{dz} \right|_{z=z_s} = \beta - \frac{1}{2N} \sum_{\mathbf{k}} \frac{1}{z_s - \frac{1}{2}v_{\mathbf{k}}} - \frac{\lambda^2}{4\beta(z_s - \frac{1}{2}v_0)^2} = 0. \quad (2.18)$$

The phase transition occurs when the saddle-point coincides with the branch point; that is, when $z_s = v_0/2$. Accordingly, we may study the neighborhood of the transition by using the expansion (2.15). Equation (2.18) becomes

$$\beta - B + \frac{3}{2}C(z_s - \frac{1}{2}v_0)^{1/2} + \dots - \frac{\lambda^2}{4\beta(z_s - \frac{1}{2}v_0)^2} = 0. \quad (2.19)$$

Clearly, we can have $z_s = v_0/2$ only when $\lambda = 0$, in which case, we have

$$1/kT_c = \beta_c = B. \quad (2.20)$$

The reader is referred to Berlin and Kac¹ for a more complete and rigorous version of this analysis.

The main point of interest here is that the magnetization curve contains no metastable region. To see

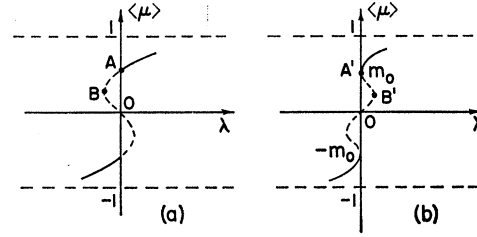


FIG. 1. Magnetization curves for (a) the infinite dimensional (infinite range) model, (b) the spherical model.

this, we compute the average spin $\langle \mu \rangle$ ¹²:

$$\begin{aligned} \langle \mu \rangle &= \lim_{N \rightarrow \infty} \left(\frac{1}{N} \frac{\partial \ln Z_0}{\partial \lambda} \right) = \frac{dF(z_s, \lambda)}{d\lambda} \\ &= \frac{\partial F}{\partial \lambda} = \frac{\lambda}{2\beta(z_s - \frac{1}{2}v_0)}, \end{aligned} \quad (2.21)$$

where we have employed the stationarity of F with respect to z at the saddle point. The relevant features of the $\langle \mu \rangle$ versus λ curve may be obtained from (2.19) for λ and $z_s - v_0/2$ sufficiently small. It is most convenient to solve for λ as a function of $\langle \mu \rangle$:

$$\lambda \cong (8\beta^3/9C^2) \langle \mu \rangle [\langle \mu \rangle^2 - ((\beta - \beta_c)/\beta)]^2. \quad (2.22)$$

This function is plotted in Fig. 1(b). For comparison, we show in Fig. 1(a) the analogous curve for, say, the infinite dimensional model.^{7,13} Note that the differential susceptibility $d\langle \mu \rangle/d\lambda$ at A in Fig. 1(a) is finite and remains positive in the metastable region AB . For the spherical model, on the other hand, the susceptibility is infinite at A' and is negative in $A'B'$, implying that the analytic continuation of the magnetization curve cannot represent a physical region.

The lack of a metastable state also shows up clearly when one examines the analytic properties of Z_0 in the complex λ plane. These properties are of interest in themselves because it is important to verify that the spherical model is consistent with the general theorems of Yang and Lee¹⁴ concerning condensing systems. We simply state the results here and relegate the detailed analysis to Appendix A.

In accord with Yang and Lee, it turns out that $Z_0(\lambda)$ has zeros along the imaginary λ axis, that is, along the unit circle in the plane of the fugacity variable e^λ . These zeros become indefinitely dense as N increases until, in the limit $N \rightarrow \infty$, the locus of zeros becomes a branch cut. It has been conjectured that, if one first takes the limit $N \rightarrow \infty$ and then continues analytically from, say, positive to negative values of λ , that one will

¹² We write $\langle \mu \rangle$ rather than m to emphasize that here we mean an average over the grand ensemble which contains a spread in values of total magnetization.

¹³ T. L. Hill, *Statistical Mechanics* (McGraw-Hill Book Company, Inc., New York, 1956), Chap. 7 and Appendix 9.

¹⁴ C. N. Yang and T. D. Lee, *Phys. Rev.* **87**, 404 (1952).

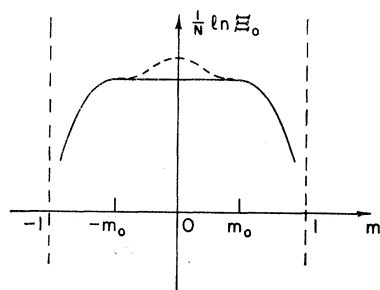


FIG. 2. Logarithm of the canonical partition function for the spherical model. The dotted line denotes the analytic continuation of the smooth function into the region $m^2 < m_0^2$.

find a smooth continuation onto the second sheet. Such a continuation does exist for Temperley's model,⁵ where the continued function may be unambiguously identified with the free energy for a metastable phase. Furthermore, the first analytic singularity encountered along the negative λ axis clearly locates the limit of metastability. What happens in the spherical model, as shown in the Appendix, is that this analytic singularity occurs at the origin in the λ plane, i.e., it lies on the locus of zeros of Z_0 .

To complete the discussion of the unmodified spherical model, we review the calculation of the canonical partition function.³ This is easily obtained by deleting λ in the second line of Eq. (2.10) and noting that the extra delta function in (2.3) implies

$$\sigma_{0,1} = N^{1/2} m. \quad (2.23)$$

Thus

$$\Xi_0(m) = \frac{\beta}{4\pi i} e^{-N/2} (2\beta)^{-N/2} \int_{-i\infty}^{i\infty} dz \exp\{N\chi_0(z, m)\}, \quad (2.24)$$

where

$$\chi_0(z, m) = \beta z - \beta(z - \frac{1}{2}v_0)m^2 - \frac{1}{2N} \sum_{\mathbf{k} \neq 0} \ln(z - \frac{1}{2}v_{\mathbf{k}}). \quad (2.25)$$

The saddle-point equation is

$$\beta(1 - m^2) = \frac{1}{2N} \sum_{\mathbf{k} \neq 0} \frac{1}{z_s - \frac{1}{2}v_{\mathbf{k}}} \\ \cong \beta_c - \frac{3C}{2} (z_s - \frac{1}{2}v_0)^{1/2} + \dots \quad (2.26)$$

Equation (2.26) has a solution $z_s > v_0/2$ only if m is greater than the spontaneous magnetization m_0 :

$$m^2 > m_0^2 = (\beta - \beta_c)/\beta, \quad (2.27)$$

which checks with (2.22) in that m_0^2 is equal to $\langle \mu \rangle^2$ when $\lambda = 0$. In this case,

$$(1/N) \ln \Xi_0 \approx -\frac{1}{2} - \frac{1}{2} \ln 2\beta + \chi_0(z_s, m). \quad (2.28)$$

When $m^2 < m_0^2$, however, the peak along the path of

steepest descent in the z plane occurs at $z = v_0/2$. Thus

$$(1/N) \ln \Xi_0 \approx -\frac{1}{2} - \frac{1}{2} \ln 2\beta + \frac{1}{2} \beta v_0 \\ - \frac{1}{2N} \sum_{\mathbf{k} \neq 0} \ln \left(\frac{v_0 - v_{\mathbf{k}}}{2} \right), \quad (2.29)$$

which is completely independent of m . It follows that the canonical free energy is a concave function with a flat top, as shown in Fig. 2. The dotted line in that figure corresponds to the dotted portion of Fig. 1(b) and represents the analytic function which is obtained by using the saddle-point equation (2.26) for all m , i.e., by forgetting that the saddle point has left the physical sheet for $m^2 < m_0^2$. Again, it is clear that the dotted portions of Figs. 1 and 2 are of no physical significance.

III. PHASE SEPARATION AND THE QUARTIC PERTURBATION

There are two possible explanations for the lack of a physically sensible analytic continuation of the partition function for the spherical model. One is that analytic continuation does not necessarily have anything to do with supersaturation. That is, the spherical model may supersaturate; but we do not know how to show this mathematically. It should be remembered that the only soluble models which have succeeded in exhibiting an analytic continuation clearly identifiable with supersaturation are Temperley's model⁴ and that of Kac, Uhlenbeck, and Hemmer.⁸ Both of these involve infinite range forces and thus may be highly unrealistic in this particular respect. The only general argument in favor of identification of the analytic continuation with a metastable state is that, experimentally, passage into the supersaturated region appears to occur smoothly. The theory of phase transitions, however, is notorious for unpleasant mathematical surprises; and it seems worthwhile to insist on more conclusive arguments.

The alternative to the above possibility is that the spherical model really does not supersaturate. This second explanation leaves open the possible physical interpretation of analytic continuation; and it is this explanation that we try to confirm. We consider first some intuitive arguments.

The classic picture of the metastable state¹¹ envisions, for example, a uniform liquid at a temperature higher than the boiling point—or at a pressure lower than the vapor pressure at the given temperature. The corresponding situation for the spin system has macroscopically uniform magnetization in a direction antiparallel to the external magnetic field. Then one considers the possibility of forming a bubble of vapor or of parallel magnetization. Because the bulk free energy of vapor is assumed to be lower than that of liquid, the appearance of the bubble lowers the free energy of the system by an amount proportional to the volume of the bubble, i.e.,

r^3 where r is the bubble radius. But if there is a positive surface energy, the total free energy will include a positive term proportional to r^2 . For small enough r , $+r^2$ will dominate $-r^3$, and the bubble will tend to dissipate. There will be a critical radius, say r_c , above which the volume energy decreases faster than the surface energy increases. When, because of some fluctuation, a bubble radius exceeds r_c , the bubble will grow indefinitely; and the liquid will boil or the magnetization will flip.

The prime requisite for the above picture is that the system exhibit two distinct phases separated by a well-defined surface. More precisely, the low-energy states of given density or magnetization must exhibit phase separation. The Ising model with a finite range interaction is an ideal example of this. If we fix the magnetization, then the state of lowest energy clearly is the one in which all of the up spins are separated from all of the down spins by a surface of minimum area.

The spherical model, on the other hand, runs into a difficulty here. Because of the continuous nature of the spin variables, there is no precise distinction between two phases. A detailed statistical treatment of this is presented in Sec. VII; but it is a worthwhile exercise to perform some preliminary zero-temperature (ground-state) calculations.

Consider the problem of minimizing the energy H_0 subject to the spherical constraint and given a fixed magnetization. The variational equation is

$$(\partial/\partial\mu_1)[H_0 + \zeta \sum_1 \mu_1^2 + \nu \sum_1 \mu_1] = -\sum_{1'} v_{1,1'} \mu_{1'} + 2\zeta \mu_1 + \nu = 0, \quad (3.1)$$

where ζ and ν are Lagrange multipliers. Although it is by no means necessary here, it will be convenient to assume that μ_1 varies much more slowly than the interaction $v_{1,1'}$ so that we may replace μ_1 by a function of a continuous variable, say $\mu(\mathbf{r})$, where \mathbf{r} is measured in units of the lattice spacing. Then, using (2.13) and (2.14), we may write (3.1) as a differential equation:

$$[-v_0 - \gamma \nabla^2 + 2\zeta] \mu(\mathbf{r}) = -\nu. \quad (3.2)$$

This equation has solutions of the form

$$\mu = -\frac{\nu}{2\zeta - v_0} + A \cos\left\{\left(\frac{-2\zeta + v_0}{\gamma}\right)^{1/2} x + \delta\right\}, \quad (3.3)$$

where δ is an arbitrary phase angle and A is a constant to be determined. The variable x measures distance parallel to one of the sides of the lattice. The magnetization condition implies

$$\nu = m(v_0 - 2\zeta), \quad (3.4)$$

and periodic boundary conditions require

$$\left(\frac{-2\zeta + v_0}{\gamma}\right)^{1/2} = \frac{2\pi}{L} \times \text{integer} \equiv K, \quad (3.5)$$

L being the length of the lattice in the x direction. Finally, the spherical constraint determines the integration constant A :

$$A = [2(1 - m^2)]^{1/2}. \quad (3.6)$$

The result is

$$\mu(x) = m + [2(1 - m^2)]^{1/2} \cos(Kx + \delta). \quad (3.7)$$

It is a trivial matter to check that (3.7) really does minimize H_0 if we choose the smallest nonzero K , i.e., $K = 2\pi/L$.

Consider Eq. (3.7) first for the case $m = 0$. Instead of separating into two equal regions of up and down spins, the μ 's tend to go from positive to negative values as gradually as possible. The situation may be compared to the pure Heisenberg ferromagnet in which the Bloch wall tends to become indefinitely thick in the absence of an anisotropy field. The second point to note is that, for nonzero m , instead of dividing into unequal regions of up and down spins, the spherical model tends to become as uniform as possible. That is, the μ 's take values as close to $\mu = m$ as are consistent with the spherical constraint. Thus, equilibrium between two phases in the spherical model does not look at all the way we think it ought⁸ to look.

In order to remedy this situation, it is proposed to add to H_0 a quartic perturbation of the form

$$H' = \alpha \sum_1 \mu_1^4, \quad (3.8)$$

where α is a small positive constant. To see the qualitative effect of this term, note that some of the μ 's determined by (3.7) for the pure spherical model have magnitudes larger than unity. The term H' makes these large values of μ energetically unfavorable. Combined with the spherical constraint, H' has the effect of flattening out the peaks in the μ versus \mathbf{l} curve. This effect can be made more obvious by noting that

$$H' = \alpha \sum_1 (\mu_1^2 - 1)^2 + \alpha N \quad (3.9)$$

by virtue of the spherical constraint. In this form, H' represents a potential with symmetric minima at $\mu = \pm 1$. In the strong-coupling limit $\alpha \rightarrow \infty$, this modified spherical model should revert to the conventional Ising model. For the small values of α of interest here, H' plays the role of an anisotropy field.

The quartic perturbation (3.8), when added to H_0 in (3.1), turns Eq. (3.2) into a very interesting nonlinear differential equation:

$$-\gamma \nabla^2 \mu - (v_0 - 2\zeta) \mu + 4\alpha \mu^3 + \nu = 0. \quad (3.10)$$

The solutions of this equation are discussed in Appendix

B. The result is exactly what one expects. The energy H_0+H' is minimized subject to the constraints by taking μ equal to ± 1 to order $N^{-1/6}$ almost everywhere in the lattice. In the transition regions where μ changes from $+1$ to -1 , the function $\mu(x)$ is well approximated by

$$\mu(x) = \tanh[x(2\alpha/\gamma)^{1/2}]; \quad (3.11)$$

thus two phases are separated by a surface whose thickness d is independent of the size of the sample:

$$d \approx (\gamma/2\alpha)^{1/2}. \quad (3.12)$$

IV. DIAGRAM EXPANSION FOR THE MODIFIED SPHERICAL MODEL

We turn here to the problem of computing thermodynamic properties of the modified spherical model. The model is almost certainly not exactly soluble; and therefore we devise a diagram expansion technique.

Let us consider the grand-canonical partition function

$$Z(\lambda) = \frac{1}{A_N} \prod_1 \left(\int_{-\infty}^{\infty} d\mu_1 \right) \delta \left(\sum_1 \mu_1^2 - N \right) \times \exp \{ -\beta(H_0+H') + \lambda \sum_1 \mu_1 \}. \quad (4.1)$$

As in Sec. II, we use the integral representation (2.6) for the delta function and define the quadratic form (2.7). Then we have

$$Z(\lambda) = \frac{\beta}{2\pi i A_N} \prod_1 \left(\int_{-\infty}^{\infty} d\mu_1 \right) \int_{-\infty}^{\infty} dz \times \exp \{ N\beta z - \beta \sum_{1,1'} P_{1,1'} \mu_1 \mu_{1'} - \beta \alpha \sum_1 \mu_1^4 + \lambda \sum_1 \mu_1 \}. \quad (4.2)$$

The diagrammatic technique is based on the expansion

$$Z(\lambda) = \frac{\beta}{2\pi i A_N} \prod_1 \left(\int_{-\infty}^{\infty} d\mu_1 \right) \int_{-\infty}^{\infty} dz \exp \{ N\beta z - \beta \sum_{1,1'} P_{1,1'} \mu_1 \mu_{1'} + \lambda \sum_1 \mu_1 \} \sum_{n=0}^{\infty} \frac{1}{n!} (-\beta\alpha)^n \left(\sum_1 \mu_1^4 \right)^n$$

$$= \frac{\beta}{2\pi i A_N} \int_{-\infty}^{\infty} dz e^{N\beta z} \sum_{n=0}^{\infty} \frac{(-\beta\alpha)^n}{n!} \sum_{\mathbf{l}_1, \mathbf{l}_2, \dots, \mathbf{l}_n} I_n(\mathbf{l}_1, \mathbf{l}_2, \dots, \mathbf{l}_n), \quad (4.3)$$

where

$$I_n(\mathbf{l}_1, \mathbf{l}_2, \dots, \mathbf{l}_n) \equiv \prod_1 \left(\int_{-\infty}^{\infty} d\mu_1 \right) \exp \{ -\beta \sum_{1,1'} P_{1,1'} \mu_1 \mu_{1'} + \lambda \sum_1 \mu_1 \} \prod_{i=1}^n \mu_{\mathbf{l}_i}^4. \quad (4.4)$$

It is apparent from (4.2) that the expansion (4.3) converges, at best, only asymptotically. Accordingly, we try to re-sum this expansion before performing the z integration.

The coefficients of the expansion (4.3) may be computed most easily by evaluating, instead of I_n , the generating function

$$g_n(\xi_1, \dots, \xi_n) \equiv \prod_1 \left(\int_{-\infty}^{\infty} d\mu_1 \right) \exp \{ -\beta \sum_{1,1'} P_{1,1'} \mu_1 \mu_{1'} + \lambda \sum_1 \mu_1 + \sum_{i=1}^n \xi_i \mu_{\mathbf{l}_i} \}, \quad (4.5)$$

which is related to I_n by

$$I_n(\mathbf{l}_1, \dots, \mathbf{l}_n) = \prod_{i=1}^n \left(\frac{\partial}{\partial \xi_i} \right) g_n(\xi_1, \dots, \xi_n) \Big|_{\xi_1 = \dots = \xi_n = 0}. \quad (4.6)$$

The integrations over the μ 's in (4.5) are performed by transforming to the σ variables introduced in Eq. (2.8).

We obtain

$$g_n = \prod'_{\mathbf{k}, s=1,2} \left(\int_{-\infty}^{\infty} d\sigma_{\mathbf{k},s} \right) \exp \{ -\beta \sum'_{\mathbf{k},s} p_{\mathbf{k}} \sigma_{\mathbf{k},s}^2 + N^{1/2} \lambda \sigma_{0,1} + \sum'_{\mathbf{k},s} \sum_{i=1}^n \xi_i a_s(\mathbf{l}_i, \mathbf{k}) \sigma_{\mathbf{k},s} \}$$

$$= \left(\frac{\pi}{\beta p_0} \right)^{1/2} \exp \left\{ \frac{1}{4\beta p_0} \left[\lambda N^{1/2} + \sum_{i=1}^n \xi_i a_1(\mathbf{l}_i, 0) \right]^2 \right\} \prod'_{\substack{\mathbf{k},s \\ \mathbf{k} \neq 0}} \left(\frac{\pi}{\beta p_{\mathbf{k}}} \right)^{1/2} \exp \left\{ \frac{1}{4\beta p_{\mathbf{k}}} \left[\sum_{i=1}^n \xi_i a_s(\mathbf{l}_i, \mathbf{k}) \right]^2 \right\}$$

$$= \prod_{\text{all } \mathbf{k}} \left(\frac{\pi}{\beta p_{\mathbf{k}}} \right)^{1/2} \exp \left\{ \frac{1}{4\beta} \sum_{i,j=1}^n \xi_i \xi_j g(\mathbf{l}_i - \mathbf{l}_j) + \frac{\lambda}{2\beta p_0} \sum_{i=1}^n \xi_i + \frac{N\lambda^2}{4\beta p_0} \right\}. \quad (4.7)$$

The function $g(\mathbf{l}_i - \mathbf{l}_j)$ appearing in the final form of (4.7) is

$$g(\mathbf{l}_i - \mathbf{l}_j) = \sum'_{\mathbf{k},s} \frac{a_s(\mathbf{l}_i, \mathbf{k}) a_s(\mathbf{l}_j, \mathbf{k})}{p_{\mathbf{k}}} = \frac{1}{N} \sum_{\mathbf{k}} \frac{e^{i\mathbf{k} \cdot (\mathbf{l}_i - \mathbf{l}_j)}}{(z - \frac{1}{2} v_{\mathbf{k}})}, \quad (4.8)$$

which will play the role of an unperturbed propagator in the following analysis.

The complete expression for the partition function now reads

$$Z(\lambda) = e^{-N/2} (2\beta)^{-N/2} \frac{\beta}{4\pi i} \int_{-i\infty}^{i\infty} dz e^{NF(z,\lambda)} \sum_{n=0}^{\infty} \frac{(-\beta\alpha)^n}{n!} \sum_{\mathbf{l}_1, \mathbf{l}_2, \dots, \mathbf{l}_n} \prod_{i=1}^n \left(\frac{\partial}{\partial \xi_i} \right)^4 \times \exp \left\{ \frac{1}{4\beta} \sum_{i,j=1}^n \xi_i \xi_j g(\mathbf{l}_i - \mathbf{l}_j) + \frac{\lambda}{2\beta(z - \frac{1}{2}v_0)} \sum_{i=1}^n \xi_i \right\} \Bigg|_{\xi=0}, \quad (4.9)$$

where the function $F(z,\lambda)$ is given by Eq. (2.11).

The rules for the diagram expansion may be read directly from (4.9). The term of order n , i.e., the coefficient of α^n , gives rise to a number of diagrams, each having n labeled points $\mathbf{l}_1, \mathbf{l}_2, \dots, \mathbf{l}_n$. We draw a line (bond) between the points \mathbf{l}_i and \mathbf{l}_j for each factor $(1/2\beta)g(\mathbf{l}_i - \mathbf{l}_j)$; and we draw a line from point \mathbf{l}_i to an external field point X for each factor $\lambda/2\beta(z - \frac{1}{2}v_0)$ obtained by differentiating with respect to ξ_i in (4.9). Each point \mathbf{l}_i must have connected to it exactly four lines corresponding to the four differentiations with respect to ξ_i .

By expanding the exponential in (4.9), we note the following factors:

- (a) Each point \mathbf{l}_i contributes a factor

$$-(4!) \beta \alpha = -24\beta\alpha.$$

- (b) Each pair of points $\mathbf{l}_i, \mathbf{l}_j$ joined by m bonds contributes a factor

$$1/m! [(1/2\beta)g(\mathbf{l}_i - \mathbf{l}_j)]^m.$$

- (c) A point connected to m external field lines contributes a factor

$$\frac{1}{m!} \left[\frac{\lambda}{2\beta(z - \frac{1}{2}v_0)} \right]^m.$$

- (d) A bond closed upon itself contributes a factor

$$\frac{1}{2} (1/2\beta)g(0).$$

The complete numerical contribution of the diagram is obtained by summing over $\mathbf{l}_1, \mathbf{l}_2, \dots, \mathbf{l}_n$ and multiplying by $1/n!$.

The reduction to unlabeled diagrams takes place in the usual manner, as does the linked-cluster analysis. Associated with any unlabeled diagram there are

$$n!/S$$

different labeled diagrams, where S is the number of permutations of the points which transform the labeled diagram into itself. If a particular linked cluster Γ appears in a diagram ν_Γ times, then S will contain a factor $\nu_\Gamma!$. Summing over all ν_Γ , we obtain

$$Z(\lambda) = e^{-N/2} (2\beta)^{-N/2} \frac{\beta}{4\pi i} \int_{-i\infty}^{i\infty} dz \times \exp.N[F(z,\lambda) + \Phi(z,\lambda)], \quad (4.10)$$

where $N\Phi$ is the sum of all linked clusters. That is,

$$N\Phi = \sum_{\Gamma} (1/S_\Gamma) W_\Gamma, \quad (4.11)$$

where W_Γ is the numerical contribution of the linked diagram Γ computed according to the Rules (a) through (d), and S_Γ is the number of symmetry operations on the points which leave Γ invariant. Note that the factors $1/m!$ in (b) and (c) and the factor $\frac{1}{2}$ in (d) may be interpreted as additional symmetry factors arising from rearrangements of the bonds.

It is obvious from Eq. (4.8) that it is most convenient to compute contributions of diagrams in a Fourier representation. Accordingly, we label each bond by a wave vector \mathbf{k} and arbitrarily assign to it a direction. Associated with any such bond is a factor

$$\frac{1}{2\beta} g_{\mathbf{k}} \equiv \frac{1}{2\beta} \frac{1}{z - \frac{1}{2}v_{\mathbf{k}}}. \quad (4.12)$$

Summing over all the \mathbf{l} 's at the vertices, we obtain wave-vector conservation throughout the diagrams. In this notation, we may write for each external-field line a factor $(\lambda/2\beta)g_0$, which makes the external-field term just a special case of (6.17), necessarily with $\mathbf{k}=0$ and with a factor λ at the open end of the bond.

V. DIAGRAM RENORMALIZATION

Although strictly classical in its physical implications, the diagram expansion developed in Sec. IV looks very much like that for a quantum-mechanical many-body problem. It is, in fact, somewhat simpler. The propagators carry only wave-vector—and not energy—variables. There are no wave-vector dependent factors at the four-vertices. It also should be remarked that, unlike most lattice problems, there are no excluded-volume difficulties, i.e., no semi-invariants to worry about.

It seems very natural now to treat the perturbation expansion by the diagram-renormalization methods developed for many-body problems. An excellent formulation of these techniques has been described by Bloch¹⁵; and we base our analysis upon his work. For a variety of reasons, these methods turn out to be remarkably well suited to the present problem.

¹⁵ C. Bloch, in *Studies in Statistical Mechanics*, edited by J. deBoer and G. E. Uhlenbeck (North-Holland Publishing Company, Amsterdam, 1964), Vol. III.

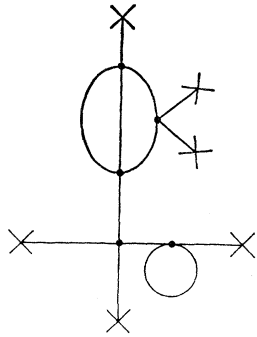


FIG. 3. A typical diagram before \mathfrak{M} renormalization.

The diagram renormalization is performed in two steps. We first eliminate all subdiagrams which are connected to the main diagram by only a single ($k=0$) line. This leads to the definition of the magnetization function \mathfrak{M} . We then perform the "self-energy" renormalization leading to the definition of the renormalized propagator \mathfrak{G}_k . We do not attempt any higher order renormalizations.

The first step is performed as follows. Given any particular diagram, for example that shown in Fig. 3, identify all of the bonds such that, if any one is broken, the diagram separates into two disconnected parts. Because all such bonds necessarily carry $k=0$, we refer to them as "0 bonds." We then may draw for the dia-

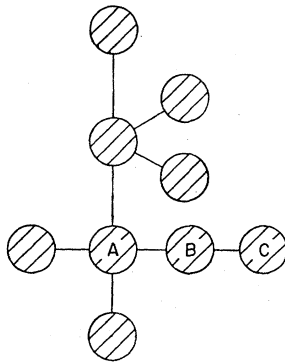


FIG. 4. The tree structure corresponding to Fig. 3.

gram an equivalent tree, that is, a diagram in which only the 0 bonds are shown explicitly. Subdiagrams containing no 0 bonds are indicated by shaded bubbles; and these bubbles are the articulation points of the tree. The tree structure corresponding to Fig. 3. is shown in Fig. 4. Note that single external field points and single four-vertices may qualify as bubbles.

The magnetization function \mathfrak{M} is defined to be the sum of the contributions of all subdiagrams which terminate in a single 0 bond. \mathfrak{M} contains the factor $(1/2\beta)g_0$, but not the factor $-4!\beta\alpha$, which will occur when \mathfrak{M} is connected into a larger diagram. The first few terms in the perturbation expansion of \mathfrak{M} are shown in Fig. 5. We see below that \mathfrak{M} is, in fact, the average magnetization of the system.

In order to express the sum of all diagrams Φ in terms of \mathfrak{M} , we use the fact that, for any tree,

$$N_B - N_A + N_L = 1, \tag{5.1}$$

where N_B is the number of bubbles, N_L is the number of lines (0 bonds), and N_A is the sum of the articulation numbers, i.e., the numbers of 0 bonds attached to the bubbles. For example, the bubble labeled A in Fig. 4 has articulation number 4; B has 2; and C has 1. Equation (5.1) may be proved easily by induction. We use this relation here to write down an expression in which each diagram is counted exactly once.

The first term in the desired expression is the sum of the contributions of all bubble diagrams¹⁶ computed by inserting a factor \mathfrak{M} for every 0 bond connected to the bubble. Let us call this term \mathfrak{D}_0 . A few leading terms

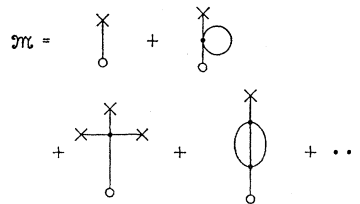


FIG. 5. Diagram expansion of the magnetization function. The small open circles represent the points at which these subdiagrams are attached to the rest of the diagram.

in \mathfrak{D}_0 are shown in Fig. 6; and the corresponding numerical contributions are as follows:

$$\mathfrak{D}_0(\mathfrak{M}) = \lambda\mathfrak{M} - \beta\alpha\mathfrak{M}^4 - (3\alpha/N)\mathfrak{M}^2 \sum_k g_k + \dots \tag{5.2}$$

It should be clear that any diagram with N_B bubbles is counted N_B times in \mathfrak{D}_0 . This is easily seen by noticing that we may find any given diagram N_B times in \mathfrak{D}_0 by basing the construction of the diagram on each of its N_B bubbles. The reader may check that symmetry factors are properly taken care of by this argument.

To complete the calculation of Φ according to (5.1) we must find expressions which count each diagram N_A and N_L times. Let us call these expressions Φ_A and Φ_L , respectively. These expressions are written most conveniently in terms of the function \mathfrak{g} , defined by

$$\mathfrak{M} = (1/2\beta)g_0\mathfrak{g}. \tag{5.3}$$

Clearly, \mathfrak{g} includes all of \mathfrak{M} , except the leading 0 bond. Equation (5.3) plays the role of the Dyson equation for 0-bond renormalization.

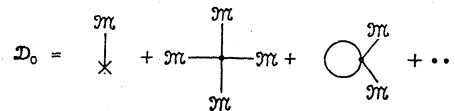


FIG. 6. Diagram expansion of the function \mathfrak{D}_0 .

¹⁶ Conventionally, these bubble diagrams are called skeletons; but we reserve the term skeleton for the diagrams which remain after self-energy renormalization.

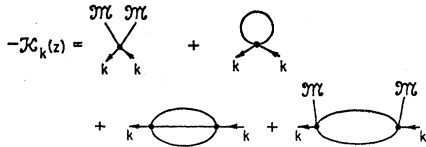


FIG. 7. Diagram expansion of the self-energy function \mathcal{K} .

Φ_A now may be written down by focussing attention on any bubble and any one of the 0 bonds attached to it. The 0 bond is part of a diagram in \mathfrak{N} . The bubble and all other factors \mathfrak{N} associated with it make a part of \mathcal{G} . For any diagram there are N_A choices of bubble plus 0 bond. Thus

$$\Phi_A = \mathfrak{N} \mathcal{G} = 2\beta g_0^{-1} \mathfrak{N}^2 \quad (5.4)$$

counts each diagram N_A times.

Similarly, Φ_L is found by basing the construction of the diagram on any of its N_L 0 bonds. Each end of the bond is attached to a subdiagram which is part of \mathcal{G} . There is now an over-all symmetry factor $\frac{1}{2}$. We have

$$\Phi_L = \frac{1}{2} (1/2\beta) g_0 \mathcal{G}^2 = \beta g_0^{-1} \mathfrak{N}^2. \quad (5.5)$$

One minor error in the above analysis must be corrected now. The diagrams summed by \mathfrak{D}_0 , Φ_A , and Φ_L include one which consists of a single 0 bond with external field factors λ at each end. The contribution of this diagram is

$$\frac{1}{2} [(1/2\beta) g_0] \lambda^2.$$

But this diagram is not really part of the perturbation expansion because it contains no α ; thus it must be

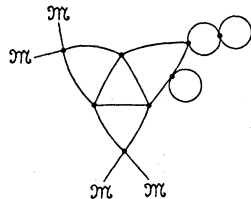


FIG. 8. A bubble diagram.

deleted from Φ . Note, however, that exactly this term appears in $F(z, \lambda)$.

Using the relation (5.1) and Eqs. (5.4) and (5.5), we write

$$\begin{aligned} \Phi &= \mathfrak{D}_0 - \Phi_A + \Phi_L - (\lambda^2/4\beta) g_0 \\ &= \mathfrak{D}_0 - \beta g_0^{-1} \mathfrak{N}^2 - (\lambda^2/4\beta) g_0. \end{aligned} \quad (5.6)$$

Then, from Eq. (4.10), we have

$$Z(\lambda) = e^{-N/2} (2\beta)^{-N/2} \frac{\beta}{4\pi i} \int_{-i\infty}^{i\infty} dz \exp\{N\Psi(z, \lambda)\}, \quad (5.7)$$

where

$$\begin{aligned} \Psi(z, \lambda) &\equiv F(z, \lambda) + \Phi(z, \lambda) = \beta z + (1/2N) \sum_k \ln g_k(z) \\ &\quad + \mathfrak{D}_0(z, \lambda, \mathfrak{N}) - \beta(z - \frac{1}{2}v_0) \mathfrak{N}^2. \end{aligned} \quad (5.8)$$

The function Ψ has a useful variational property. Suppose we consider the explicit dependence of Ψ on

\mathfrak{N} . From the diagrammatic definition of \mathfrak{D}_0 , it should be clear that

$$\partial \mathfrak{D}_0 / \partial \mathfrak{N} = \mathcal{G}. \quad (5.9)$$

Thus

$$\partial \Psi / \partial \mathfrak{N} = \mathcal{G} - 2\beta g_0^{-1} = 0, \quad (5.10)$$

according to the Dyson relation (5.3).

Equation (5.10) may be used immediately in proving the physical significance of \mathfrak{N} . In general, the integral (5.7) may be performed by the saddle-point method. Then

$$(1/N) \ln Z \approx -\frac{1}{2} - \frac{1}{2} \ln 2\beta + \Psi(z_s, \lambda), \quad (5.11)$$

where z_s is the saddle point determined by

$$\partial \Psi / \partial z = 0 \quad \text{at} \quad z = z_s. \quad (5.12)$$

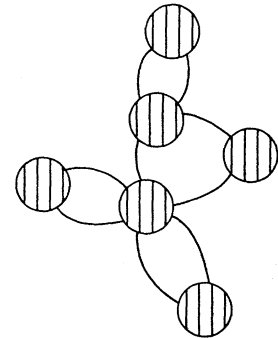


FIG. 9. The tree of cycles corresponding to Fig. 8.

The magnetization is

$$\langle \mu \rangle = d\Psi(z_s, \lambda) / d\lambda = \partial \Psi / \partial \lambda. \quad (5.13)$$

Because of Eqs. (5.10) and (5.12), we need consider only the explicit λ dependence of Ψ in (5.13). Now the only λ which occurs explicitly in Ψ appears in the term $\lambda \mathfrak{N}$ in \mathfrak{D}_0 , as given by Eq. (5.2). Thus

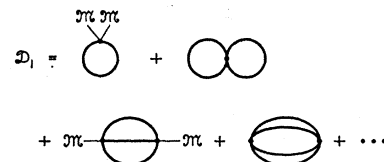
$$\langle \mu \rangle = \mathfrak{N}(z_s, \lambda). \quad (5.14)$$

The second step in the renormalization procedure is the expression of \mathfrak{D}_0 in terms of the renormalized propagator, which we call $\mathcal{G}_k(z)$. We define the self-energy function $-\mathcal{K}_k(z)$ in the usual way as the sum of contributions from the proper self-energy diagrams. The first few such diagrams are shown in Fig. 7. The relation between \mathcal{G}_k and \mathcal{K}_k is the conventional Dyson equation

$$\mathcal{G}_k(z) = [z - \frac{1}{2}v_k + \mathcal{K}_k(z)]^{-1}. \quad (5.15)$$

Our problem now is to eliminate the unperturbed propagators g_k in favor of the \mathcal{G}_k and still count every diagram just once. We do this by essentially the same

FIG. 10. Diagram expansion of the function \mathfrak{D}_1 . The heavy lines represent renormalized propagators \mathcal{G} .



trick as before. Any bubble diagram in \mathfrak{D}_0 may be resolved uniquely into a tree of self-energy cycles. For example, the diagram shown in Fig. 8 has the tree structure shown in Fig. 9. Each shaded bubble in Fig. 9 contains no self-energy cycles. The relation (5.1) still holds except that the 0 bonds are replaced by cycles. That is,

$$N_B - N_A + N_C = 1, \quad (5.16)$$

where N_C is the number of self-energy cycles and N_A is the number of cycles attached to each bubble summed over all the bubbles.

The first two diagrams contributing to \mathfrak{D}_0 shown in Fig. 6 contain no propagators g_k ; thus we may separate these out.

$$\mathfrak{D}_0 = \lambda \mathfrak{M} - \beta \alpha \mathfrak{M}^4 + \Phi_1. \quad (5.17)$$

Φ_1 now contains three terms counting the diagrams N_B , N_A , and N_C times, respectively.

Each shaded bubble in Fig. 9 contains what is commonly called a skeleton diagram, i.e., a diagram having no self-energy cycles. Let us define the function $\mathfrak{D}_1(\mathfrak{M}, \mathcal{G})$ to be the sum of the contributions of all skeleton diagrams computed by replacing g_k by \mathcal{G}_k in each line of each diagram. A few of the leading terms of \mathfrak{D}_1 are shown in Fig. 10. The renormalized propagators are indicated by heavy lines. By reasoning similar to that used before, it should be clear that \mathfrak{D}_1 counts each diagram in Φ_1 exactly N_B times.

The expression Φ_{1A} which counts each diagram N_A times is obtained by considering a single bubble and one of the self-energy cycles to which it belongs. This gives

$$\Phi_{1A} = - (1/2N) \sum_{\mathbf{k}} \mathcal{K}_{\mathbf{k}} \mathcal{G}_{\mathbf{k}}. \quad (5.18)$$

Also, it is easy to see that the sum over all cycles,

$$\begin{aligned} \Phi_{1C} &= \frac{1}{N} \sum_{n=1}^{\infty} \frac{1}{2n} \sum_{\mathbf{k}} [-g_{\mathbf{k}} \mathcal{K}_{\mathbf{k}}]^n = -\frac{1}{2N} \sum_{\mathbf{k}} \ln[1 + g_{\mathbf{k}} \mathcal{K}_{\mathbf{k}}] \\ &= -\frac{1}{2N} \sum_{\mathbf{k}} \ln g_{\mathbf{k}} + \frac{1}{2N} \sum_{\mathbf{k}} \ln \mathcal{G}_{\mathbf{k}}, \end{aligned} \quad (5.19)$$

counts each diagram N_C times.¹⁷ Finally, we use Eq. (5.16) to write

$$\Phi_1 = \mathfrak{D}_1 - \Phi_{1A} + \Phi_{1C}. \quad (5.20)$$

We now combine Eqs. (5.8), (5.17), and (5.20) to complete the renormalized form of the function:

$$\begin{aligned} \Psi(z, \lambda) &= \beta z + \frac{1}{2N} \sum_{\mathbf{k}} \ln \mathcal{G}_{\mathbf{k}}(z) \\ &+ \frac{1}{2N} \sum_{\mathbf{k}} \mathcal{K}_{\mathbf{k}} \mathcal{G}_{\mathbf{k}} - \beta (z - \frac{1}{2} v_0) \mathfrak{M}^2 \\ &+ \lambda \mathfrak{M} - \beta \alpha \mathfrak{M}^4 + \mathfrak{D}_1(\mathfrak{M}, \mathcal{G}). \end{aligned} \quad (5.21)$$

¹⁷ To be absolutely precise, we should subtract the quantity $(1/2N) \sum_{\mathbf{k}} \mathcal{K}_{\mathbf{k}} g_{\mathbf{k}}$ from both (5.18) and (5.19); but these terms cancel out in the next equation.

In analogy to Eq. (5.10), it turns out that Ψ is stationary with respect to variations of the $\mathcal{G}_{\mathbf{k}}$. To see this, write the Dyson relation (5.15) in the form

$$\mathcal{K}_{\mathbf{k}} = \mathcal{G}_{\mathbf{k}}^{-1} - g_{\mathbf{k}}^{-1}, \quad (5.22)$$

and substitute into (5.21). Then

$$2N(\partial\Psi/\partial\mathcal{G}_{\mathbf{k}}) = \mathcal{G}_{\mathbf{k}}^{-1} - g_{\mathbf{k}}^{-1} + 2N(\partial\mathfrak{D}_1/\partial\mathcal{G}_{\mathbf{k}}). \quad (5.23)$$

From the diagram expansions of $\mathcal{K}_{\mathbf{k}}$ and \mathfrak{D}_1 , we may deduce that¹⁸

$$-\mathcal{K}_{\mathbf{k}} = 2N(\partial\mathfrak{D}_1/\partial\mathcal{G}_{\mathbf{k}}); \quad (5.24)$$

thus

$$\partial\Psi/\partial\mathcal{G}_{\mathbf{k}} = 0. \quad (5.25)$$

It should be noted that, by virtue of (5.25), Eq. (5.9) becomes

$$g = \lambda - 4\beta\alpha\mathfrak{M}^3 + \partial\mathfrak{D}_1/\partial\mathfrak{M}, \quad (5.26)$$

where the function $\mathcal{G}_{\mathbf{k}}$ is to be held fixed during the differentiation with respect to \mathfrak{M} . The stationarity property (5.10) and magnetization relation (5.14) clearly are unmodified.

VI. FIRST-ORDER DIAGRAMS AND THE MAGNETIZATION CURVE

We propose now to compute \mathfrak{D}_1 to first order in α and then work through the formalism as outlined above.

The numerical contributions of the first two diagrams in Fig. 10 are

$$\begin{aligned} \mathfrak{D}_1 &= - (3\alpha/N) \mathfrak{M}^2 \sum_{\mathbf{k}} \mathcal{G}_{\mathbf{k}}(z) \\ &- 3\beta\alpha [(1/2\beta N) \sum_{\mathbf{k}} \mathcal{G}_{\mathbf{k}}]^2. \end{aligned} \quad (6.1)$$

All other diagrams are higher order in α . From Eq. (5.26) we obtain an equation for the magnetization function:

$$\begin{aligned} g &= \lambda - 4\beta\alpha\mathfrak{M}^3 + (\partial\mathfrak{D}_1/\partial\mathfrak{M}) \\ &= \lambda - 4\beta\alpha\mathfrak{M}^3 - (6\alpha\mathfrak{M}/N) \sum_{\mathbf{k}'} \mathcal{G}_{\mathbf{k}'}(z). \end{aligned} \quad (6.2)$$

The self-energy function is determined by Eq. (5.24):

$$\begin{aligned} +\mathcal{K}_{\mathbf{k}} &= -2N(\partial\mathfrak{D}_1/\partial\mathcal{G}_{\mathbf{k}}) \\ &= +6\alpha\mathfrak{M}^2 + (3\alpha/\beta N) \sum_{\mathbf{k}'} \mathcal{G}_{\mathbf{k}'}. \end{aligned} \quad (6.3)$$

Note that the right-hand side of (6.3) is independent of \mathbf{k} in this first-order approximation. We shall call this \mathbf{k} -independent self-energy function simply $\mathcal{K}(z)$. Together with the Dyson relations (5.3) and (5.15), Eqs. (6.2) and (6.3) determine self-consistently the renormalized quantities \mathfrak{M} and $\mathcal{G}_{\mathbf{k}}$.

It is clear from what follows that the path of steepest descent in the z plane does, in fact, pass across a single

¹⁸ The factor 2 arises from symmetry under the transformation $\mathbf{k} \rightarrow -\mathbf{k}$.

saddle point z_s on the physical sheet of the function Ψ . The stationarity equations (5.10) and (5.25) make the saddle-point condition particularly simple:

$$d\Psi/dz = \beta - (1/2N) \sum_{\mathbf{k}} \mathcal{G}_{\mathbf{k}}(z) - \beta \mathfrak{M}^2 = 0 \text{ at } z = z_s. \quad (6.4)$$

Equation (6.4) is formally exact to all orders in α because \mathfrak{D}_1 contains no explicit z dependence.

Inserting the saddle-point condition (6.4) into Eq. (6.3), we find

$$\mathfrak{K}(z_s) = 6\alpha. \quad (6.5)$$

The renormalized propagator now becomes

$$\mathcal{G}_{\mathbf{k}}(z_s) = [z_s - \frac{1}{2}v_{\mathbf{k}} + 6\alpha]^{-1}. \quad (6.6)$$

It should be apparent that the quantity

$$\Delta_s \equiv z_s - \frac{1}{2}v_0 + 6\alpha \quad (6.7)$$

is playing the role of an energy gap in the spectrum of states described by $\mathcal{G}_{\mathbf{k}}(z_s)$. Note:

$$\mathcal{G}_{\mathbf{k}}(z_s) = [\Delta_s + \frac{1}{2}(v_0 - v_{\mathbf{k}})]^{-1} \cong (\Delta_s + \frac{1}{2}\gamma k^2)^{-1}, \quad (6.8)$$

according to Eq. (2.14). We also may write

$$(1/2N) \sum_{\mathbf{k}} \mathcal{G}_{\mathbf{k}}(z_s) \cong \beta_c - (3C/2)\Delta_s^{1/2} + \dots, \quad (6.9)$$

where we have used Eq. (2.15). The quantity β_c is the critical temperature for the unmodified spherical model as given in Eq. (2.20).

By inserting Eq. (6.9) into (6.4), we obtain a relation between the energy gap and the magnetization:

$$\Delta_s^{1/2} \cong (2\beta/3C) \{ \mathfrak{M}^2 - [(\beta - \beta_c)/\beta] \}. \quad (6.10)$$

Then, if we use (6.9) and (6.10) in Eqs. (6.2) and (6.3), we may eliminate Δ_s to find

$$\lambda \cong (8\beta^3/9C^2) \mathfrak{M} \{ \mathfrak{M}^2 - [(\beta - \beta_c)/\beta] \}^2 - 8\alpha\beta \mathfrak{M}^3. \quad (6.11)$$

This equation is to be compared with Eq. (2.22) for the pure spherical model, which is identical to (6.11) when $\alpha = 0$.

At high temperatures, $\beta \ll \beta_c$, the perturbation correction in (6.11) makes little noticeable change in the magnetization curve. Below the critical temperature, however, (6.11) gives the magnetization curve shown in Fig. 11. The crucial point is that this curve, in contrast to Fig. 1(b), exhibits a section AB which presumably indicates supersaturation. This is exactly what we hoped would be the effect of the quartic perturbation according to the discussion in Sec. III.

On the other hand, there are some very unpleasant features of Eq. (6.11). In particular, its behavior near the critical temperature is not physically sensible. Curves for $\beta = \beta_c$ and a special value of $\beta \lesssim \beta_c$ are shown in Fig. 12. The trouble is that the spontaneous magnetization computed at point A in Fig. 11 does not go to zero at $\beta = \beta_c$. In fact, this solution of the equation $\lambda = 0$ simply disappears at a finite value of \mathfrak{M} at some

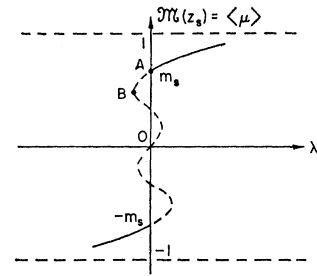


FIG. 11. Magnetization curve for the modified spherical model for β appreciably larger than β_c .

temperature $\beta < \beta_c$. Conventionally one looks for small values of \mathfrak{M} near the critical temperature; that is, one would approximate (6.11) by

$$\lambda \cong (8\beta^3/9C^2) [(\beta - \beta_c)/\beta]^2 \mathfrak{M}, \quad (6.12)$$

which is just the spherical model with a singularity in the susceptibility at $\beta = \beta_c$. But in our modified problem, the region of (6.11) for $\mathfrak{M} \sim 0$ is clearly the part of the curve where the saddle-point method is not valid.

The fact of the matter is that any simple truncation of the perturbation expansion for \mathfrak{D}_1 loses its validity sufficiently close to the critical point. Quite generally, the critical point seems to occur when the energy gap Δ_s vanishes. In the pure spherical model, the gap goes to zero as we approach T_c from above, and remains zero below T_c . With the quartic perturbation, the gap opens up again below T_c , as we see immediately below.¹⁹ The limitation on the perturbation method follows from the fact that it is effectively Δ_s , which we are expanding in powers of α . If the renormalized equations require Δ_s to be small of order, say, α^2 near some $\beta \cong \beta_c$, then we know that Eq. (6.7) cannot adequately describe such behavior.

At this point we may determine which parts of the magnetization curves described by Eq. (6.11) represent accurate solutions for the model system. We do this simply by requiring that Δ_s , as determined by Eq. (6.10), be no smaller than order α . Let us check first that point A, the beginning of the supersaturation curve in Fig. 11, satisfies this self-consistency criterion. For $\lambda = 0$ and $\mathfrak{M} \neq 0$, we solve Eq. (6.11) and insert it into (6.10) to find

$$\Delta_s \cong 4\alpha \mathfrak{M}^2. \quad (6.13)$$

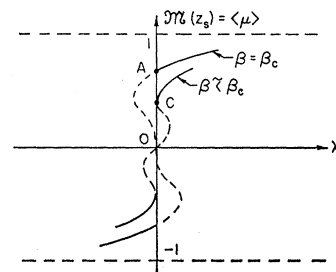


FIG. 12. Magnetization curves for the modified spherical model for $\beta = \beta_c$ and a particular value of $\beta \lesssim \beta_c$.

¹⁹ A very similar mathematical phenomenon occurs in the exact solution of the two-dimensional Ising model. See the discussion given by Berlin and Kac in the reference cited in footnote 1.

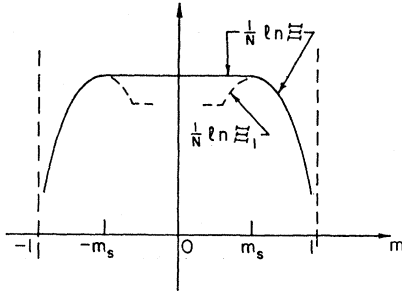


FIG. 13. Logarithm of the canonical partition function for the modified spherical model. The dotted line denotes the function $(1/N) \ln \Xi_1$, computed according to Eqs. (7.3) and (7.4).

If β is greater than β_c by a finite amount, independent of α , then we know that the spontaneous magnetization, say m_s , satisfies

$$m_s = \mathfrak{M}(\lambda=0) \cong [(\beta - \beta_c)/\beta]^{1/2} + O(\alpha); \quad (6.14)$$

thus Δ_s remains of order α . We conclude that, at sufficiently low temperatures, the supersaturation effect computed here is real. In contrast, we may compute Δ_s at point A in Fig. 12, i.e., at $\beta = \beta_c$. From Eq. (6.11) we have

$$m_s^2(\beta = \beta_c) = \mathfrak{M}^2(\lambda=0, \beta = \beta_c) = (9C^2/\beta^2)\alpha, \quad (6.15)$$

which implies in (6.13) that $\Delta_s \propto \alpha^2$. A similar result ($\Delta_s \propto \alpha^2$) pertains at point C in Fig. 12 where the temperature is slightly higher than T_c . These results give us some assurance that the physically unreasonable behavior near the critical point is a feature of the mathematical approximations and not the model itself.

VII. TWO-PHASE REGION

In order to study the two-phase region, we must work in the canonical rather than the grand canonical ensemble. This turns out to be not quite so simple as it may look at first sight; and we see that the formalism developed so far requires some modification before it may be used to describe two distinct phases in equilibrium. The naive calculation is of some interest in itself, however; so we proceed with that first.

Presumably, in order to compute the partition function at a fixed total magnetization Nm , we need only set $\lambda=0$ and $\sigma_{0,1} = mN^{1/2}$ in computing the generating function \mathcal{G}_n in Eq. (4.7). That is:

$$\mathcal{G}_n(m) = e^{-N\beta[z - (v_0/2)]m^2} \prod_{k \neq 0} \left(\frac{\pi}{\beta \rho_k} \right)^{1/2} \times \exp \left\{ \frac{1}{4\beta} \sum_{i,j=1}^n \xi_i \xi_j g'(\mathbf{l}_i - \mathbf{l}_j) + m \sum_i \xi_i \right\}, \quad (7.1)$$

where

$$g'(\mathbf{l}_i - \mathbf{l}_j) = \frac{1}{N} \sum_{k \neq 0} \frac{e^{i\mathbf{k} \cdot (\mathbf{l}_i - \mathbf{l}_j)}}{z - \frac{1}{2}v_k}. \quad (7.2)$$

The summation of renormalized diagrams proceeds now just as before, except that we must replace each \mathfrak{M} by m and sum only skeleton diagrams with no $\mathbf{k}=0$ lines. We shall see that the quantity computed in this manner is not quite the correct canonical partition function Ξ .

In order to avoid confusion, let us call this function Ξ_1 . Explicitly,

$$\Xi_1(m) = e^{-N/2(2\beta)^{-N/2}} \frac{\beta}{4\pi i} \int_{-i\infty}^{i\infty} dz \exp\{N\chi(z, m)\}, \quad (7.3)$$

where

$$\chi(z, m) = \beta z - \beta(z - \frac{1}{2}v_0)m^2 + \frac{1}{2N} \sum_{k \neq 0} \ln \mathcal{G}_k(z) + \frac{1}{2N} \sum_{k \neq 0} \mathcal{K}_k \mathcal{G}_k - \beta \alpha m^4 + \mathcal{D}_1(m, \mathcal{G}). \quad (7.4)$$

χ is stationary with respect to \mathcal{G}_k ; therefore the saddle-point equation is simply

$$\beta(1 - m^2) = (1/2N) \sum_{k \neq 0} \mathcal{G}_k(z_s). \quad (7.5)$$

This equation should be compared with Eq. (2.26) for the unmodified spherical model. Note that (7.5) is exact to all orders in α .

The trouble with Eq. (7.5) is that it implies an anomaly in the function $(1/N) \ln \Xi_1(m)$ at a value of m such that z_s is the singular point of the right-hand side of (7.5). But this singularity must be associated with the vanishing of the energy gap in the propagator \mathcal{G}_k ²⁰; and we know that the gap is finite of order α at $m = m_s$. It is easy to convince oneself that the anomaly in $(1/N) \ln \Xi_1(m)$ as determined by Eqs. (7.3) and (7.4) occurs at the end of the supersaturation curve, more or less as shown by the dotted line in Fig. 13.

This mysterious result—a calculation of the supersaturation curve when we expected a flat-topped function describing two phases in equilibrium—is easier to understand physically than it is mathematically. Physically, it is clear that the system in the two-phase region is unstable in a nonuniform external field. That is, an infinitesimal nonuniform field will produce a macroscopic spatial variation of the magnetization; and we should allow for this in the calculation. Before pursuing this idea further, however, a few words should be said about the mathematical pathology encountered here. How does it happen that the perturbation expansion, which, according to the discussion of the last section, is convergent near $m = m_s$, gives a qualitatively wrong answer?

The first part of the explanation is that the calculation outlined above is really not canonical but grand

²⁰ A more detailed analysis of the renormalization equations based on the first-order diagrams in \mathcal{D}_1 shows that the right-hand side of (7.5) becomes singular when the energy gap is of order α^2 , i.e., at a place where the renormalization procedure is not self-consistent.

canonical. Comparing Eqs. (5.21) and (7.4), we can write

$$(1/N) \ln \Xi_1(m) = (1/N) \ln Z(\lambda) - \lambda m, \quad (7.6)$$

where m is related to λ by

$$m = \frac{1}{N} \frac{d \ln Z(\lambda)}{d \lambda}. \quad (7.7)$$

The point is that, as soon as we try to compute the canonical free energy by the present perturbation expansion, then, term by term in the expansion, this function $(1/N) \ln \Xi_1$ is identical to the expansion of the Legendre transform (7.6) of the grand-canonical potential. Now the paradox is that, no matter what the exact $\ln \Xi(m)$ looks like, the Legendre transform of $\ln Z(\lambda)$ is always a convex function—in fact, the convex envelope of $\ln \Xi(m)$. This was emphasized in a previous paper by the author in collaboration with Bloch.⁷ The function $(1/N) \ln \Xi_1$ shown in Fig. 13, however, clearly is not convex. This is related to a second conclusion of the previous paper,⁷ namely, that the perturbation expansion does not define $(1/N) \ln \Xi_1$ in the two-phase region but may converge (asymptotically) to an entirely different function, perhaps the free energy of the metastable state. This is just what we seem to find here.

Let us return now to the more physical point of view for calculation of the canonical partition function. The argument about instability in a nonuniform field is best illustrated by a preliminary calculation with the unmodified spherical model. Suppose we compute the partition function in the presence of an external field of the form

$$-\epsilon \sum_1 \mu_1 \cos \mathbf{K} \cdot \mathbf{I}, \quad |\mathbf{K}| = 2\pi/L. \quad (7.8)$$

The point to be demonstrated is that, if we let ϵ vanish at the end of the calculation—after we have taken the limit $N \rightarrow \infty$ —the magnetization does not revert to a uniform distribution.

The partition function of interest is

$$\begin{aligned} \Xi_0(m, \epsilon) = & \frac{1}{A_N} \prod_1 \left(\int_{-\infty}^{\infty} d\mu_1 \right) \delta \left(\sum_1 \mu_1^2 - N \right) \delta \left(\sum_1 \mu_1 - Nm \right) \\ & \times \exp \{ -\beta H_0 + \epsilon \sum_1 \mu_1 \cos \mathbf{K} \cdot \mathbf{I} \}. \end{aligned} \quad (7.9)$$

This may be evaluated by previously described techniques. One finds

$$\begin{aligned} \Xi_0(m, \epsilon) = & e^{-N/2} (2\beta)^{-N/2} \frac{\beta}{4\pi i} \int_{-i\infty}^{i\infty} dz \\ & \times \exp \{ N \chi_0(z, m, \epsilon) \}, \end{aligned} \quad (7.10)$$

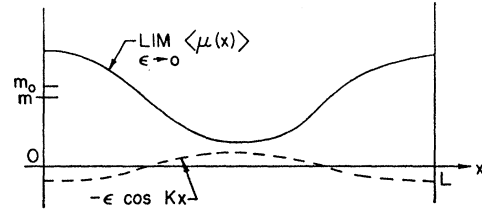


FIG. 14. A typical magnetization distribution for the spherical model in the two-phase region.

where

$$\begin{aligned} \chi_0(z, m, \epsilon) = & \beta z - \beta \left(z - \frac{1}{2} v_0 \right) m^2 \\ & - \frac{1}{2N} \sum_{\mathbf{k} \neq 0} \ln \left(z - \frac{1}{2} v_{\mathbf{k}} \right) + \frac{\epsilon^2}{8\beta \left(z - \frac{1}{2} v_{\mathbf{k}} \right)}. \end{aligned} \quad (7.11)$$

The average magnetization is

$$\begin{aligned} \langle \mu_1 \rangle = & m + \frac{2}{N} \left(\frac{\partial \ln \Xi_0(m, \epsilon)}{\partial \epsilon} \right) \cos \mathbf{K} \cdot \mathbf{I} \\ \approx & m + \frac{\epsilon}{2\beta \left(z_s - \frac{1}{2} v_0 \right)} \cos \mathbf{K} \cdot \mathbf{I}, \end{aligned} \quad (7.12)$$

where z_s is the saddle point and we have let $v_{\mathbf{k}} \rightarrow v_0$ as $N = L^3 \rightarrow \infty$. The saddle-point equation is

$$\begin{aligned} \beta(1 - m^2) = & \frac{1}{2N} \sum_{\mathbf{k} \neq 0} \frac{1}{z_s - \frac{1}{2} v_{\mathbf{k}}} + \frac{\epsilon^2}{8\beta \left(z_s - \frac{1}{2} v_0 \right)^2} \\ \cong & \beta_c - (3C/2) \left(z_s - \frac{1}{2} v_0 \right)^{1/2} + \frac{\epsilon^2}{8\beta \left(z_s - \frac{1}{2} v_0 \right)^2}. \end{aligned} \quad (7.13)$$

If m^2 is greater than $m_0^2 = 1 - \beta_c/\beta$ (the spontaneous magnetization), then $z_s - \frac{1}{2} v_0$ remains finite as $\epsilon \rightarrow 0$ and

$$\lim_{\epsilon \rightarrow 0} \left[\frac{\epsilon}{2\beta \left(z_s - \frac{1}{2} v_0 \right)} \right] = 0. \quad (7.14)$$

On the other hand, if $m^2 < m_0^2$, then $z_s \rightarrow v_0/2$ as $\epsilon \rightarrow 0$. From the second line of (7.13) we have

$$\begin{aligned} \lim_{\epsilon \rightarrow 0} \left[\frac{\epsilon}{2\beta \left(z_s - \frac{1}{2} v_0 \right)} \right] = & \pm \left[2 \left(1 - m^2 - \frac{\beta_c}{\beta} \right) \right]^{1/2} \\ = & \pm [2(m_0^2 - m^2)]^{1/2}. \end{aligned} \quad (7.15)$$

If $\epsilon \rightarrow +0$, the plus sign is appropriate; thus

$$\lim_{\epsilon \rightarrow +0} \langle \mu_1 \rangle = m + [2(m_0^2 - m^2)]^{1/2} \cos \mathbf{K} \cdot \mathbf{I}. \quad (7.16)$$

This function is illustrated in Fig. 14. Note that the ground-state calculation (3.7) is just a special case of this result.

We now wish to repeat this sort of calculation for the modified spherical model. It is expected that there will be some qualitative differences.

Inserting the nonuniform external field (7.8) into the generating function \mathcal{G}_n , we find, instead of (7.1),

$$\mathcal{G}_n(m, \epsilon) = \exp \left\{ -N\beta \left(z - \frac{1}{2}v_0 \right) m^2 + \frac{N\epsilon^2}{8\beta \left(z - \frac{1}{2}v_K \right)} \right\} \\ \times \prod_{\mathbf{k} \neq 0} \left(\frac{\pi}{\beta p_{\mathbf{k}}} \right)^{1/2} \exp \left\{ m \sum_i \xi_i + \frac{\epsilon}{2\beta p_{\mathbf{K}}} \sum_i \xi_i \cos \mathbf{K} \cdot \mathbf{I}_i \right. \\ \left. + \frac{1}{4\beta} \sum_{i,j} \xi_i \xi_j g'(\mathbf{I}_i - \mathbf{I}_j) \right\}, \quad (7.17)$$

where g' is again defined by (7.2); i.e., no $\mathbf{k}=0$ lines may appear in the diagrams. The rules for the diagram expansion again may be read from (7.17) by looking for the various terms which can be generated by differentiating (7.17) with respect to the ξ 's. The important new feature is that the nonuniform external field [generated by $(\epsilon/2\beta p_{\mathbf{K}}) \sum_i \xi_i \cos \mathbf{K} \cdot \mathbf{I}_i$ in (7.17)] now must be attached in all possible ways to the diagrams.

This has the effect that the magnetization function, constructed according to the obvious topological recipe as illustrated in Fig. 5, must be allowed to carry all wave vectors \mathbf{k} which may be generated by various insertions of the external field. Furthermore, the renormalized propagator \mathcal{G} is no longer diagonal in the wave-vector subscripts.

There is no real difficulty in formally repeating the renormalization program for the diagrams generated by (7.17). We denote the magnetization function by $\mathfrak{M}_{\mathbf{k}}$ with the supplementary definition

$$\mathfrak{M}_{\mathbf{k}=0} \equiv m. \quad (7.18)$$

The Dyson relation analogous to (5.3) is

$$\mathcal{G}_{\mathbf{k}} = 2\beta \left(z - \frac{1}{2}v_{\mathbf{k}} \right) \mathfrak{M}_{\mathbf{k}}. \quad (7.19)$$

The renormalized propagator is a matrix $\mathcal{G}_{\mathbf{k}, \mathbf{k}'}$; and the corresponding self-energy matrix is defined by

$$\mathcal{K}_{\mathbf{k}, \mathbf{k}'} = (\mathcal{G}^{-1})_{\mathbf{k}, \mathbf{k}'} - \left(z - \frac{1}{2}v_{\mathbf{k}} \right) \delta_{\mathbf{k}, \mathbf{k}'}. \quad (7.20)$$

Now

$$\Xi(m, \epsilon) = e^{-N/2} (2\beta)^{-N/2} \frac{\beta}{4\pi i} \int_{-i\infty}^{i\infty} dz \exp \{ N\chi(z, m, \epsilon) \}, \quad (7.21)$$

where

$$\chi(z, m, \epsilon) = \beta z + \frac{1}{2N} \sum_{\mathbf{k} \neq 0} (\ln \mathcal{G})_{\mathbf{k}, \mathbf{k}} + \frac{1}{2N} \sum_{\mathbf{k}, \mathbf{k}'} \mathcal{K}_{\mathbf{k}, \mathbf{k}'} \mathcal{G}_{\mathbf{k}, \mathbf{k}'} - \beta \sum_{\mathbf{k}} \left(z - \frac{v_{\mathbf{k}}}{2} \right) \mathfrak{M}_{\mathbf{k}}^2 \\ - \beta \alpha \sum_{\mathbf{k}_1, \mathbf{k}_2, \mathbf{k}_3, \mathbf{k}_4} \mathfrak{M}_{\mathbf{k}_1} \mathfrak{M}_{\mathbf{k}_2} \mathfrak{M}_{\mathbf{k}_3} \mathfrak{M}_{\mathbf{k}_4} \delta_{\mathbf{k}_1 + \mathbf{k}_2 + \mathbf{k}_3 + \mathbf{k}_4, 0} + \mathcal{D}_1(\mathfrak{M}, \mathcal{G}) + \epsilon \mathfrak{M}_{\mathbf{K}}. \quad (7.22)$$

The reader should have no difficulty in generalizing (7.22) from (7.4).

The renormalization equations are

$$\mathcal{G}_{\mathbf{k}} = \epsilon \delta_{\mathbf{k}, \mathbf{K}} - 4\beta \alpha \sum_{\mathbf{k}_1, \mathbf{k}_2, \mathbf{k}_3} \mathfrak{M}_{\mathbf{k}_1} \mathfrak{M}_{\mathbf{k}_2} \mathfrak{M}_{\mathbf{k}_3} \delta_{\mathbf{k}_1 + \mathbf{k}_2 + \mathbf{k}_3, \mathbf{k}} + \partial \mathcal{D}_1 / \partial \mathfrak{M}_{\mathbf{k}}, \quad \mathbf{k} \neq 0; \quad (7.23)$$

and

$$\mathcal{K}_{\mathbf{k}, \mathbf{k}'} = -2N \frac{\partial \mathcal{D}_1}{\partial \mathcal{G}_{\mathbf{k}, \mathbf{k}'}}. \quad (7.24)$$

These equations again imply stationarity of χ with respect to variations of $\mathfrak{M}_{\mathbf{k}}$ and $\mathcal{G}_{\mathbf{k}, \mathbf{k}'}$. It should be emphasized, however, that (7.23) is not necessarily valid for $\mathbf{k}=0$, and that χ is not necessarily stationary with respect to variations of $\mathfrak{M}_{\mathbf{k}} \equiv m$. Making use of the stationarity property, the saddle-point equation may be written

$$(1/2N) \sum_{\mathbf{k}} \mathcal{G}_{\mathbf{k}, \mathbf{k}}(z) = \beta \left(1 - \sum_{\mathbf{k}} \mathfrak{M}_{\mathbf{k}}^2 \right). \quad (7.25)$$

Our problem is to find out under what conditions the set of equations (7.23), (7.24), and (7.25) will have nontrivial solutions in the limit $\epsilon \rightarrow 0$. The trivial solution is, of course,

$$\mathfrak{M}_{\mathbf{k}} = 0, \quad \mathbf{k} \neq 0, \quad (7.26)$$

which brings us back to Eq. (7.4) and the partition

function Ξ_1 . It should be apparent now that, in computing Ξ_1 from Eqs. (7.3) and (7.4), we have constrained the ensemble so that the average magnetization of the system must be uniform. This is why we believe that, for $m^2 < m_s^2$, Ξ_1 describes the supersaturated state.

A new class of solutions of Eqs. (7.23)–(7.25) is possible under the condition that m has a value such that it is consistent with Eq. (7.23) for $\mathbf{k}=0$. This new class of solutions coincides with the trivial solution (7.26) when $m = m_s$. To see this, note that if in (7.23) we set $\mathbf{k}=0$, $\epsilon=0$, and $\mathfrak{M}_{\mathbf{k}} = \mathfrak{M}_{\mathbf{k}, 0}$, we obtain exactly Eq. (6.2) for $\lambda=0$. This equation, in conjunction with (7.24) and (7.25) which now are identical to (6.3) and (6.4), is satisfied by $\mathfrak{M} = m_s$.

Under the assumption that (7.23) is satisfied for $\mathbf{k}=0$, it is most convenient to write the basic equations in the \mathbf{I} rather than \mathbf{k} representation. Let us again choose

for \mathcal{D}_1 the first-order diagrams, i.e., the first two shown in Fig. 10. In the \mathbf{l} representation, these are

$$\mathcal{D}_1 \cong - (3\alpha/N) \sum_{\mathbf{l}} \mathfrak{M}^2(\mathbf{l}) \mathcal{G}(\mathbf{l}, \mathbf{l}) - 3\beta\alpha \left[(1/2\beta N) \sum_{\mathbf{l}} \mathcal{G}(\mathbf{l}, \mathbf{l}) \right]^2. \quad (7.27)$$

For slow variations of μ_1 we replace \mathbf{l} by the continuous variable \mathbf{r} and let

$$v_{\mathbf{k}} \rightarrow v_0 + \gamma \nabla^2, \quad (7.28)$$

as in Sec. III. Then Eqs. (7.23)–(7.25) become, respectively,

$$\mathcal{J}(\mathbf{r}) = 2\beta \left[z - \frac{1}{2}v_0 - \frac{1}{2}\gamma \nabla^2 \right] \mathfrak{M}(\mathbf{r}) = \epsilon \cos \mathbf{K} \cdot \mathbf{r} - 4\beta\alpha \mathfrak{M}^3(\mathbf{r}) - 6\alpha \mathfrak{M}(\mathbf{r}) \mathcal{G}(\mathbf{r}, \mathbf{r}); \quad (7.29)$$

$$\mathcal{K}(\mathbf{r}, \mathbf{r}') = \mathcal{K}(\mathbf{r}) \delta(\mathbf{r} - \mathbf{r}') = \delta(\mathbf{r} - \mathbf{r}') \left[6\alpha \mathfrak{M}^2(\mathbf{r}) + (3\alpha/\beta) \mathcal{G}(\mathbf{r}, \mathbf{r}) \right]; \quad (7.30)$$

$$\frac{1}{2N} \int d^3r \mathcal{G}(\mathbf{r}, \mathbf{r}) = \beta \left(1 - \frac{1}{N} \int \mathfrak{M}^2(\mathbf{r}) d^3r \right). \quad (7.31)$$

Note that (7.31) does not depend on the approximation (7.27).

If we divide Eq. (7.29) by β , set $\epsilon=0$, and identify $z=\zeta$, then this equation looks very much like Eq. (3.10), which described the ground state of this system. Indeed, in the limit $\beta \rightarrow \infty$, the equations are identical.²¹ We know from Appendix B that there are solutions of (7.29) in which $\mathfrak{M}(\mathbf{r})$ has constant magnitude almost everywhere in the lattice. This assumption of constant magnitude greatly simplifies the remaining analysis. Note that in Eq. (7.31) we can write

$$\frac{1}{N} \int \mathfrak{M}^2(\mathbf{r}) d^3r = \mathfrak{M}_s^2 + O(N^{-1/3}), \quad (7.32)$$

where \mathfrak{M}_s is the constant magnitude of $\mathfrak{M}(\mathbf{r})$ and the correction $O(N^{-1/3})$ comes from integrating over the surfaces where $\mathfrak{M}(\mathbf{r})$ goes from $-\mathfrak{M}_s$ to $+\mathfrak{M}_s$. By the same sort of argument, the function $\mathcal{G}(\mathbf{r}, \mathbf{r})$ will be independent of \mathbf{r} , except perhaps in the immediate neighborhood of a surface.

It should be obvious that the relevant value of the constant \mathfrak{M}_s is just m_s , which is the rigorous solution of the equations for $\epsilon=0$ and completely uniform $\mathfrak{M}(\mathbf{r})$. We may achieve any value of $m^2 < m_s^2$ by dividing the system into a finite number of domains in which $\mathfrak{M}(\mathbf{r}) = \pm m_s$. The particular domain configuration will be determined by energy minimization in the vanishing nonuniform external field, for example, as is shown in Fig. 15. It is essential that the number of domains is independent of N and that the volume of each domain

²¹ The quantity ν which appears in Eq. (3.10) vanishes exponentially as $N \rightarrow \infty$, and therefore does not appear in (7.29). See Appendix B.

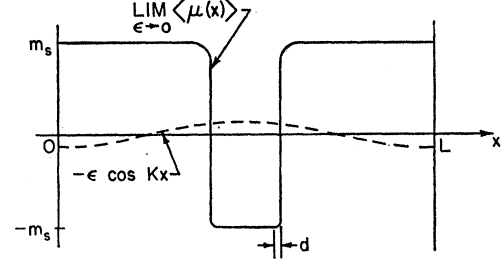


FIG. 15. Magnetization distribution for the modified spherical model under conditions the same as those which produced the distribution shown in Fig. 14 for the pure spherical model.

becomes infinite as N goes to infinity. This process leaves the saddle-point equation (7.31) unchanged to order $N^{-1/3}$, and therefore leaves z_s fixed. Furthermore, notice that $\chi(z, m, \epsilon=0)$ in Eq. (7.22) depends only on $\mathfrak{M}^2(\mathbf{r})$. Therefore, in the two-phase region bounded by $m = \pm m_s$, the function $(1/N) \ln \Xi(m)$ remains constant to order $N^{-1/3}$. The complete function is shown in Fig. 13.

The shape of the surface at finite temperature may be computed if we make the approximation that $\mathcal{G}(\mathbf{r}, \mathbf{r})$ is constant everywhere, including the inside of the surface region. Denote this constant simply by \mathcal{G} and set $\mathfrak{M}^2(\mathbf{r}) = m_s^2$ in Eq. (7.30). Then we have

$$\frac{1}{2} \mathcal{G} = \frac{1}{2N} \sum_{\mathbf{k}} \left(z_s - \frac{v_0}{2} + \frac{\gamma}{2} k^2 + 6\alpha m_s^2 + \frac{3\alpha}{\beta} \mathcal{G} \right)^{-1} \cong \beta \epsilon - (3C/2) \Delta_s^{1/2} + \dots, \quad (7.33)$$

where

$$\Delta_s = z_s - (v_0/2) + 6\alpha m_s^2 + (3\alpha/\beta) \mathcal{G}. \quad (7.34)$$

The quantity that we wish to evaluate is the coefficient of the linear term in $\mathfrak{M}(\mathbf{r})$ in Eq. (7.29). This is just

$$z_s - (v_0/2) + (3\alpha/\beta) \mathcal{G} = \Delta_s - 6\alpha m_s^2. \quad (7.35)$$

Then, from Eq. (6.13), we have

$$z_s - (v_0/2) + (3\alpha/\beta) \mathcal{G} = -2\alpha m_s^2. \quad (7.36)$$

Equation (7.29) for $\epsilon=0$ becomes

$$-\gamma \nabla^2 \mathfrak{M} - 4\alpha \mathfrak{M}^3 - 4\alpha m_s^2 \mathfrak{M} = 0. \quad (7.37)$$

Referring to Appendix B, we obtain, for the variation of \mathfrak{M} perpendicular to a plane surface,

$$\mathfrak{M}(x) = m_s \tanh[m_s (2\alpha/\gamma)^{1/2} x]. \quad (7.38)$$

The temperature dependence is contained in the quantity m_s and seems quite reasonable; i.e., the surface thickness d increases as the temperature rises:

$$d(\beta) \cong [1/m_s(\beta)] (\gamma/2\alpha)^{1/2}. \quad (7.39)$$

VIII. DISCUSSION

We have shown that the addition of a weak anisotropy field to the spherical model produces a very complete and realistic mathematical picture of a first-

order phase transition. The canonical free energy, and correspondingly the isotherm for the equivalent lattice gas, has a flat section in the two-phase region. The analytic continuation of the free energy into the two-phase region seems to describe a metastable state.

The work presented here is incomplete in at least two respects, however. First, we have not been able to study the model near the critical point because the diagram renormalization technique develops internal inconsistencies. Perhaps identification of the problem, as in Sec. VI, will become the first step toward its solution.

The second shortcoming has to do with the metastable phase. The discussion presented here seems to the author to be intuitively appealing but not really rigorous. A more convincing argument might involve the solution of a time-dependent problem, e.g., a calculation of the motion of the system as one changes the magnetic field in various ways. This would get us involved, however, in the most difficult sort of irreversible statistical mechanics. It seems likely that progress can be made short of such an ambitious project. For example, should not the critical radius r_c introduced in Sec. III show up somewhere in the formalism? The mathematical difficulties involved in discussing the limit of metastability, however, are probably the same as those which arise near the critical point. In any case, it will be interesting to see if something better can be done.

APPENDIX A

Analytic Properties of the Partition Function for the Spherical Model

We wish to examine $Z_0(\lambda)$, defined by Eqs. (2.10) and (2.11), as a function of the complex variable λ . In the following analysis, we evaluate the integral over z in (2.10) by the method of steepest descent. Accordingly, a contour map of $\text{Re}F(z, \lambda)$ in the z plane is shown in Fig. 16. The map is drawn here for a small, real value of λ and $\beta > \beta_c$. In drawing this picture, we have taken the limit $N \rightarrow \infty$ in (2.11) and used the approximation (2.15). This procedure is legitimate, even for studying the dependence of Z_0 on large N , as long as the saddle points are not close of order $(1/N)$ to the locus of points $z = v_k/2$, i.e., the branch cut in F . The algebra required for drawing Figs. 16 and 17 is perfectly straightforward and is not reproduced here.

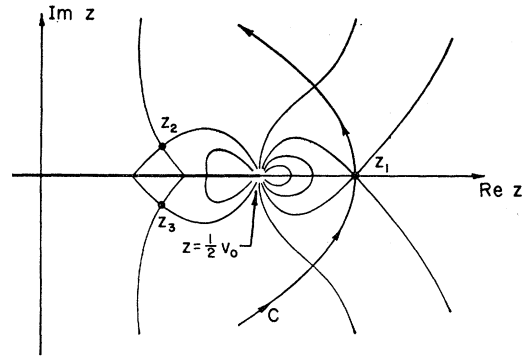


FIG. 16. Contour map of $\text{Re}F(z, \lambda)$ for λ real and β appreciably greater than β_c .

Note that in Fig. 16 there are three saddle points on the physical sheet, here labeled z_1, z_2 , and z_3 . The path of steepest descent C passes through z_1 ; thus

$$(1/N) \ln Z_0(\lambda) \approx -\frac{1}{2} - \frac{1}{2} \ln 2\beta + F(z_1). \quad (A1)$$

Let us now move λ counterclockwise around a small circle centered at the origin in the λ plane and observe the resulting variations in the z plane. The saddle

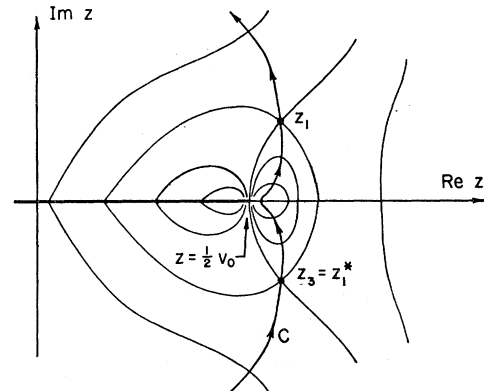


FIG. 17. Contour map of $\text{Re}F(z, \lambda)$ for λ pure imaginary.

points move roughly counterclockwise around the branch point $z = v_0/2$. As λ approaches the imaginary axis, z_2 disappears through the branch cut and z_1 and z_3 move to complex conjugate positions, as shown in Fig. 17. Because both saddle points z_1 and z_3 now lie on the same level line, the integration contour must pass through both. In this case, we have

$$Z_0(i|\lambda|) \approx \frac{\beta}{4\pi} e^{-N/2} (2\beta)^{-N/2} \left(\frac{2\pi}{N|F''(z_1)|} \right)^{1/2} \{ e^{-i\delta + NF(z_1)} + e^{i\delta + NF^*(z_1)} \} \\ = \frac{\beta}{2\pi} e^{-N/2} (2\beta)^{-N/2} \left(\frac{2\pi}{N|F''(z_1)|} \right)^{1/2} e^{+N \text{Re}F(z_1)} \cos[N \text{Im}F(z_1) - \delta], \quad (A2)$$

where

$$\delta = \frac{1}{2} \arg F''(z_1). \quad (A3)$$

The cosine factor implies that Z_0 oscillates rapidly along the imaginary axis in the λ plane; thus the imaginary axis is the locus of the Yang-Lee zeros.

As λ crosses the imaginary axis, the dominant saddle point suddenly becomes z_3 . The limit function

$$\lim_{N \rightarrow \infty} \frac{1}{N} \ln Z_0(\lambda) \quad (\text{A4})$$

is therefore nonanalytic across the imaginary axis.

Suppose that, instead of computing this function, we consider (A1) for λ to the right of the imaginary axis, take the limit $N \rightarrow \infty$, and *then* continue analytically in λ into the left-hand half-plane. Clearly, this analytic continuation is obtained by using (A1) and following z_1 as we continue to move λ . That is, we evaluate $Z_0(\lambda)$ as if we had made a mistake and chosen the wrong saddle point. When λ has completed a half-circle and returned to the real axis, z_1 has moved around to the position formerly occupied by z_2 ; z_3 is now the dominant saddle point at the former position of z_1 ; and a fourth saddle point, previously out of sight on an unphysical sheet, has replaced z_3 . In the notation of Fig. 16, the function obtained by this analytic continuation is

$$-\frac{1}{2} - \frac{1}{2} \ln 2\beta + F(z_2). \quad (\text{A5})$$

The important point is that z_2 and $F(z_2)$ are complex. Furthermore, had we moved λ clockwise around the circle, we should have obtained

$$-\frac{1}{2} - \frac{1}{2} \ln 2\beta + F(z_3) = -\frac{1}{2} - \frac{1}{2} \ln 2\beta + F^*(z_2). \quad (\text{A6})$$

These results are correct no matter how small we choose $|\lambda|$ after taking $N \rightarrow \infty$. Thus the function defined as the analytic continuation of (A4) starting from the right-hand half λ plane has a branch point at $\lambda=0$. If we choose the branch cut to lie along the negative real axis, then the discontinuity across the cut is $2i \operatorname{Im} F(z_2)$.

APPENDIX B

Solutions of the Nonlinear Magnetization Equation (3.10)

Without loss of generality, we may assume that μ varies in only one direction, say the x direction. Then Eq. (3.10) becomes

$$\gamma(d^2\mu/dx^2) = (2\zeta - v_0)\mu + 4\alpha\mu^3 + \nu. \quad (\text{B1})$$

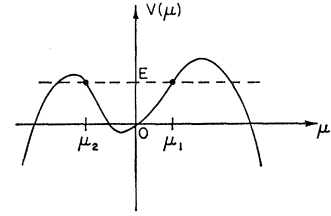
The solutions of this equation are easily found, if we interpret them as describing the motion in time x of a particle of mass γ , position μ , subject to the conservative force given by the right-hand side of (B1). The energy integral is

$$\frac{1}{2}\gamma(d\mu/dx)^2 = -V(\mu) + E, \quad (\text{B2})$$

where

$$-V(\mu) = (\zeta - \frac{1}{2}v_0)\mu^2 + \alpha\mu^4 + \nu\mu. \quad (\text{B3})$$

FIG. 18. The potential $V(\mu)$ which appears in Eq. (B3).



A typical function $V(\mu)$ is shown in Fig. 18. The solutions of interest are those in which the particle executes bounded, periodic motion between μ_1 and μ_2 .

We immediately may discard those solutions of (B1) for which a quadratic (harmonic) approximation to (B3) is valid. Such solutions would be identical to those for the unmodified spherical model as given by Eq. (3.7). But the energy is minimized for such solutions by choosing $\zeta - \frac{1}{2}v_0 \rightarrow 0$ as $N \rightarrow \infty$, which is inconsistent with neglecting $\alpha\mu^4$ in (B3).

A more nearly correct solution to (B1) may be found by choosing ν , ζ , and E such that $dV/dx=0$ at $\mu_1 = -\mu_2 = 1$. That is,

$$\begin{aligned} \zeta &= \frac{1}{2}v_0 - 2\alpha, \\ E &= \alpha, \\ \nu &= 0. \end{aligned} \quad (\text{B4})$$

Equation (B2) becomes

$$d\mu/dx = \pm (2\alpha/\gamma)^{1/2}(\mu^2 - 1). \quad (\text{B5})$$

The solution of (B5) is

$$\mu(x) = \pm \tanh[x(2\alpha/\gamma)^{1/2}]. \quad (\text{B6})$$

Here the two peaks of $V(\mu)$ are symmetric. The particle sits indefinitely long on one peak, moves to the other in a time of order $(\gamma/2\alpha)^{1/2}$, and then stays indefinitely long on the second peak.

The actual solution that we want is one in which the particle stays a long but finite time Δx of order N in the neighborhood of each peak. Such a solution may be constructed by making small changes in the parameters (B4) so that the particle never quite reaches the top of either peak. Also, by choosing ν different from zero we may make the particle spend more time near one peak than the other, thus adjusting the value of m . The required changes in ζ , E , and ν turn out to be extremely small for large N ; in fact they go to zero exponentially in the limit $N \rightarrow \infty$. It follows that the parameters (B4) characterize exactly the infinite volume solution of the magnetization problem. Note that the finite temperature values of these parameters come out of the formalism automatically in the derivation of Eq. (7.37).